Beyond RSRP: A Sensing-Assisted Handover Framework in V2I Networks

Yunxin Li*, Fan Liu†, Christos Masouros‡
*Southern University of Science and Technology, Shenzhen, China
†Southeast University, Nanjing, China
‡University College London, London, UK
liyx2022@mail.sustech.edu.cn, f.liu@ieee.org, c.masouros@ucl.ac.uk

***Abstract*—Given the challenges of high mobility and frequent handovers in 5G NR's vehicle-to-infrastructure (V2I) communications, the Integrated Sensing and Communications (ISAC) technique, now recognized in IMT-2030 as a usage scenario, is introduced to boost mobile network efficiency. Leveraging this emerging paradigm, our study delves into a V2I network within the 5G NR context, proposing a sensing-assisted handover mechanism that integrates ISAC to refine the inter-cell handover process. This mechanism uses precise beamforming and kinematic parameter estimation to reduce signaling and interruption time in inter-cell handover process. This approach enables a distance-based handover triggering mechanism that is both proactive and information-rich, allowing the serving gNB to inform the target gNB of the vehicle's location preemptively. Numerical results from link-level simulations at a crossroad scenario demonstrate that this sensing-assisted handover mechanism enables faster triggering and reduces the interruption time by 76.46%, while enhancing communication performance.**

***Index Terms*—V2I, ISAC, 5G NR, inter-cell handover.**

I. Introduction

In the realm of intelligent transportation, Vehicle-to-Everything (V2X) networks, facilitated by the next-generation cellular systems, 5G-Advanced (5G-A) and 6G, are set to play a transformative role. The V2X networks are expected to enable seamless and intelligent interaction among vehicles and their surrounding environment, including infrastructure (V2I), pedestrians (V2P) and networks (V2N), creating a fully interconnected transportation ecosystem. This technology leverages the high-speed, low-latency characteristics of 5G to support a wide range of applications, from autonomous driving and traffic efficiency to safety and environmental sustainability.

Two potential solutions to support V2X communications, Dedicated Short-Range Communications (DSRC) and cellular Vehicle-to-Everything (C-V2X), each present their unique challenges [1]. DSRC, which operates on a lower dedicated frequency band, suffers from a lower communication rate. The allocated DSRC spectrum may not meet the high data traffic demand for in-vehicle internet access, which is expected to be dominated by data-intensive video applications. Furthermore, DSRC's performance may be compromised in high mobility scenarios due to the small coverage range, leading to an increased number of handovers. On the other hand, C-V2X, especially in its network mode, faces the traditional handover challenges associated with cellular networks. High-speed vehicles necessitate rapid handover decisions to maintain seamless connectivity. This process can be complicated by rapidly changing signal quality, influenced by various factors such as obstacles, weather conditions, and vehicular traffic. Moreover, frequent handovers can result in increased signaling overhead and potential service disruptions.

Addressing the aforementioned challenges, Integrated Sensing and Communications (ISAC) has been identified as a promising solution [2], recognized for its ability to concurrently perform active sensing and communication functions with the aid of massive multi-input-multi-output (mMIMO) antenna array and millimeter wave (mmWave) technology inherent in 5G NR. More notably, by using the sensing information to design communication beamforming in real time, *sensing-assisted communications* has revealed the coordination gain in ISAC systems.

Previous research in this field has predominantly focused on the development of beam tracking and positioning algorithms to minimize the reliance on pilot signals, thereby improving communication performance. Established predictive methods, such as the Extended Kalman Filter (EKF) [3] and message passing algorithm [4], have been widely used. More recent studies have proposed algorithms designed to tackle tracking challenges associated with extended targets [5] and intricate road geometries [6]. However, these methods, despite their well-crafted design, typically assume a simplistic frame structure and do not account for adaptivity in concurrent protocol. Furthermore, recent efforts to optimize handover, either by designing Rx beamforming [7] or using a multi-armed bandit to select the optimal gNB [8], have overlooked the potential of ISAC-enabled systems.

To bridge this research gap, we propose a 5G NR sensing-assisted handover frame structure and protocol. We construct a simulation environment using ray-tracing method considering both line-of-sight (LoS) and non-LoS (NLoS) paths at a crossroad. Numerical results demonstrate a reduction in triggering time and interruption time, as well as an overall enhanced communication performance.

II. Classic Handover in NR

This section primarily focuses on the inter-cell handover process in NR, which pertains to the transition of data session from one cell to another. This mechanism is particularly

vital in mobile environments, where user mobility necessitates frequent changes in the serving cell.

A. Frame Structure

In the 5G NR connected state, the Discontinuous Reception (DRX) cycle is widely adopted to conserve energy. The DRX cycle, delineated in TS 38.331 by the 3GPP [9], comprises two primary phases: "On Duration" and "Off Duration". During the DRX-OnDuration, the UE actively transmits downlink and uplink data with the serving gNB (s-gNB) and monitors reference signals from other gNBs to prepare for potential handovers. Conversely, during the DRX-OffDuration, the UE ceases reception and monitoring activities.

For the purposes of this study, we assume a DRX cycle with a period of 10ms, equivalent to the duration of an NR FR2 radio frame. The first half of the DRX cycle is assigned as the DRX-OnDuration, and the second half as the DRX-OffDuration.

During the DRX-OnDuration, the UE monitors the Synchronization Signal (SS) burst, which is the most common reference signal used in handover process. The SS burst is composed of multiple Synchronization Signal Blocks (SSBs) and can have varying periods in NR. However, the most frequently used period is assumed to be 20ms. Although up to 64 SSBs can be transmitted within an SS burst, this can result in significant overhead. Consequently, only a portion of the SSBs are typically transmitted in each SS burst period to cover the serving area.

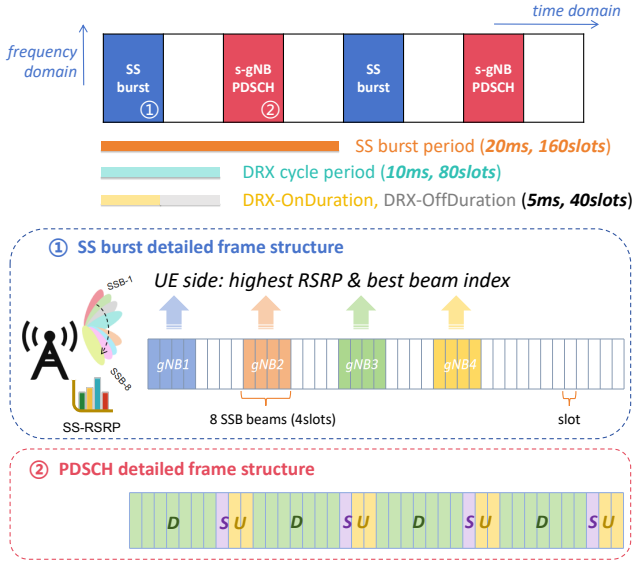

Fig. 1. Adopted Frame Structure

As shown in Fig. 1, we adopt a widely adopted 5G NR frame structure, denoted as "DDDDDDDSUU". Here, "D", "S", and "U" represent the downlink slot, special slot (with guard period), and uplink slot, respectively. We assume that the Demodulation Reference Signal (DMRS) in the Physical Downlink Shared Channel (PDSCH) adopts the mapping type "A", with an additional DMRS added due to the high mobility inherent in V2I networks. The general throughput of the communication system can be written as:

$$\text{Throughput (in Mbps)} = 10^{-6} \cdot \left(N_{\text{Layers}} \cdot Q_{\text{M}} \cdot \frac{N_{\text{PRB}} \cdot 12}{T_{\text{s}}} \cdot (1 - \text{BER} - \text{OH}) \right) \tag{1}$$

where N_{Layers}, Q_{M}, N_{PRB}, T_{s} denote the number of layers in MIMO, modulation order, number of practical resource blocks, and the average OFDM symbol duration, respectively. Moreover, BER and OH represent the bit error rate and the overhead percentage.

Thus, based on frame structure in Fig. 1, each SS burst period comprises two DRX cycles. The first DRX-OnDuration is dedicated to measuring the SSBs as reference signals from neighboring gNBs and maintaining synchronization with the s-gNB. The second DRX-OnDuration is utilized for PDSCH transmission, during which downlink and uplink data are exchanged between the s-gNB and UE. This mechanism ensures not only efficient data transmission with the s-gNB but also continuous monitoring for potential handovers in NR networks, particularly in dynamic V2I scenarios.

B. Triggering Event and Handover Command

In accordance with the TS 38.331 up to Release 17.4.0 [9], a total of 17 triggering events for handover have been delineated, of which six (namely Event A1-A6) pertain to intra-RAT (Radio Access Technology) events. These events are predicated upon the periodic measurement reports of reference signals and uplink reports. Among these, Event A3 is mostly prevalently employed. The triggering condition for Event A3 is instantiated when the performance of reference signals of a neighboring cell surpasses that of the serving cell by a predetermined offset. The gNB that satisfies the triggering condition is defined as the target gNB (t-gNB).

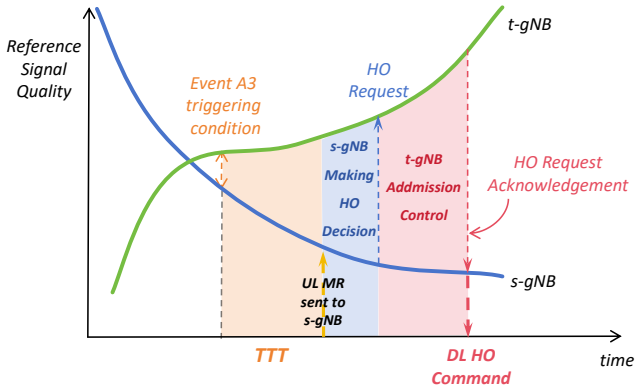

Fig. 2. Event-A3 Triggered Handover

To obviate the occurrence of so-called ping-pong handovers, characterized by incessant and unnecessary toggling between cells, the uplink measurement report of the t-gNB is dispatched to the s-gNB subsequent to a specified Time-to-Trigger (TTT)

duration, as explicitly defined in TS 38.331. Multiple configurations of TTT is specified to adapt in different scenarios.

The handover decision is made by the s-gNB after it receives the uplink measurement report (MR) after TTT, which subsequently transmits a handover request to the t-gNB. The s-gNB then awaits an acknowledgement of the handover request, predicated on the admission control at the t-gNB. This admission control is a prerequisite to ascertain that the t-gNB possesses the requisite resources to accommodate the incoming UE. Consequently, the handover command is issued from the s-gNB to the UE, thereby instigating the process of transitioning the UE to the t-gNB.

C. Interruption Time

The interruption time during conventional handover is of paramount importance as it signifies a temporary suspension of both downlink and uplink data transmission between the UE and the s-gNB. The commencement of this interruption is triggered by the handover command, marking the onset of a complex, multi-stage process that contributes significantly to the overall latency of the handover. Detailed components of the interruption time are presented in Table.I.

TABLE I
COMPONENTS OF INTERRUPTION TIME

Components	Time
RRC processing delay	10ms
Fine time tracking and acquiring full timing information of the t-gNB T_{Δ}	SMTC (max)
UE processing $T_{\text{processing}}$	20ms (max)
Interruption uncertainty T_{IU}	170ms (max)
msgA (PRACH)	1 or 2 slots
msgB-ResponseWindow	320 slots (max)
msgB (RAR)	1 or 2 slots
RRC Reconfiguration Complete	8 slots

The initial stage of this process is characterized by the Radio Resource Control (RRC) reconfiguration delay [9], which is an indispensable latency that allows the UE's hardware and software to adjust to the new configuration parameters dispatched by the s-gNB. Upon RRC reconfiguration, the UE initiates a complex process of fine time tracking and synchronization with the t-gNB. This process hinges on the successful reception of SSBs from the t-gNB, which convey crucial timing and frequency information. The duration of this stage should be shorter than the SSB-based Measurement Timing Configuration (SMTC) period [10]. After achieving synchronization by SSB post-processing, the UE conducts RF retuning, baseband retuning, and security updates. It then proceeds to the 2-step contention-free RACH procedure (CFRA), typically used in handovers to minimize interruption. This process commences with an initial message transmission (msg-A), succeeded by a waiting period for the first PRACH slot. Notably, the UE maps the PRACH occasion to the SSB block, transmitting the PRACH at the corresponding occasion tied to the optimal beam, thus enabling the t-gNB to identify the chosen SSB beam. This waiting period, influenced by the PRACH configuration period, configuration index, and selected optimal SSB beam, is termed as interruption uncertainty T_{IU}. Within a specified response window, the UE is expected to receive the random access response (RAR), also known as message-B (msg-B), which contains the uplink resource grant and the timing advance command information. The procedure concludes when the UE transmits an RRC reconfiguration complete message to the t-gNB, signaling a successful handover, terminating the interruption interval, and establishing the t-gNB as the new s-gNB.

III. SENSING-ASSISTED HANDOVER IN NR

Traditional handover mechanisms, which rely primarily on the transmission of reference signals and their corresponding uplink reports, often result in substantial overhead and increased interruption time. To address these limitations, this section proposes a novel sensing-assisted handover in the NR V2I network. The goal is to minimize unnecessary signaling and reduce interruption time. We assume that all gNBs in neighboring cells operate in the NR FR2 frequency band and are equipped with half-wavelength uniform planar arrays (UPAs). Each gNB features N_t transmit antennas and N_r receive antennas. The vehicle, equipped with a UPA of M receive antennas and currently in connected mode with the s-gNB via both LoS and NLoS channels, is traversing a crossroad shown in Fig.3. The vehicle's key kinematic parameters at the nth time slot include the azimuth and elevation angle $\boldsymbol{\theta}_n = [\theta_n, \phi_n]^T$, range d_n and velocity v_n. These are assumed to remain constant within each time slot, as the slot duration is shorter than the communication channel's coherence time.

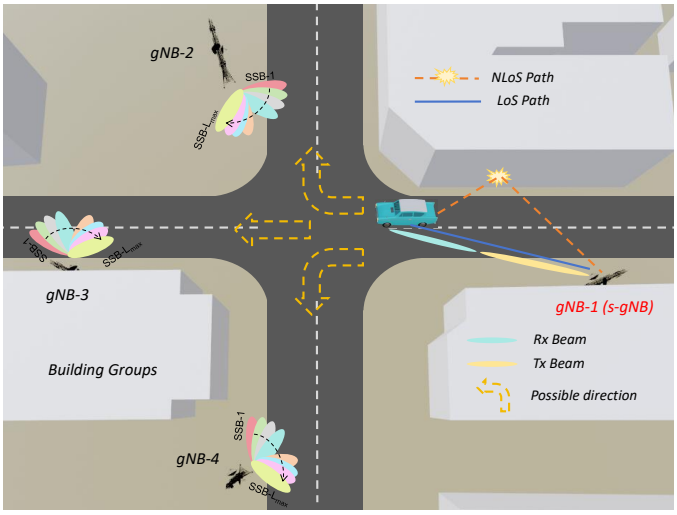

Fig. 3. Simulation scenario

A. System Model

Consider the nth time slot, where the received communication signal from the s-gNB at the UE side is given by:

$$c_n(t) = \sqrt{pN_tM}\sum_{k=1}^{K}\alpha_{k,n}\mathbf{v}_n^T\mathbf{u}(\boldsymbol{\theta}_{k,n})\mathbf{a}^T(\boldsymbol{\theta}_{k,n})\mathbf{f}_n s_n(t) + z_c(t) \tag{2}$$

In this equation, $s_n(t)$ denotes the transmitted OFDM signal, and p denotes the transmitted signal power. The steering vectors of the gNB and UE are represented by $\mathbf{a}(\boldsymbol{\theta}_{k,n})$ and $\mathbf{u}(\boldsymbol{\theta}_{k,n})$, respectively. The transmit and receive beamforming vectors of gNB and UE are denoted by $\mathbf{f}_n$ and $\mathbf{v}_n$, respectively. $z_c(t)$ stands for the Gaussian noise term.

The s-gNB receives reflected echoes from the LoS path and $K-1$ scatterers of NLoS paths, which can be expressed as:

$$\mathbf{r}_n(t) = \sqrt{pN_tN_r}\sum_{k=1}^{K}\beta_{k,n}e^{j2\pi\mu_{k,n}t}\mathbf{b}(\boldsymbol{\theta}_{k,n})\mathbf{a}^T(\boldsymbol{\theta}_{k,n}) \cdot\mathbf{f}_n s_n(t-\tau_{k,n}) + \mathbf{z}_r(t) \tag{3}$$

where $\mathbf{b}(\boldsymbol{\theta}_{k,n})$ is the receive steering vector for the gNB. Here, $\mu_{k,n}$ and $\tau_{k,n}$ denote the Doppler frequency and the time delay of the kth scatterer, respectively, which are related to the radial velocity $v_{k,n}$ and relative distance $d_{k,n}$. Given the complex radar cross-section (RCS) $\epsilon_{k,n}$, the reflection coefficient can be expressed as $\beta_{k,n} = \epsilon_{k,n}(2d_{k,n})^{-2}$. Finally, $\mathbf{z}_r(t)$ denotes the complex additive white Gaussian noise with zero mean.

The steering vector of UPA, $\mathbf{a}(\boldsymbol{\theta}_{k,n})$, is expressed as:

$$\mathbf{a}(\boldsymbol{\theta}_{k,n}) = \sqrt{\frac{1}{N_{t,x}N_{t,y}}}\left[1,\cdots,e^{j\pi(N_{t,x}-1)\sin\theta\cos\phi}\right]^T \otimes \left[1,\cdots,e^{j\pi(N_{t,y}-1)\sin\phi}\right]^T \tag{4}$$

where θ and ϕ are the azimuth and elevation angles, while $N_{t,x}$ and $N_{t,y}$ denote the number of antennas in each row and column of the UPA, respectively. The beamforming vector at the nth slot $\mathbf{f}_n$ is designed based on the predicted angle $\hat{\boldsymbol{\theta}}_{n|n-1}$ from the $(n-1)$th slot as:

$$\mathbf{f}_n = \mathbf{a}(\hat{\boldsymbol{\theta}}_{n|n-1}) \tag{5}$$

B. Kalman Filter Tracking

In the context fo vehicle movement at crossroads, the state evolution model for straight roads proposed in [3] is not directly applicable. Given the uncertainty of vehicle movement at intersections (i.e., the vehicle may go straight, turn left or right), we propose a more generalized state evolution model:

$$\begin{cases} \theta_n = \theta_{n-1} + w_\theta \\ \phi_n = \phi_{n-1} + w_\phi \\ d_n = d_{n-1} - v_{n-1}\Delta T + w_d \\ v_n = v_{n-1} + w_v \end{cases} \tag{6}$$

This model does not rely on specific road geometry and is thus applicable to any vehicle trajectory. The state evolution model and the corresponding measurement model can be compactly expressed as:

$$\begin{cases} \text{State Evolution Model: } \boldsymbol{\Upsilon}_n = \mathbf{g}(\boldsymbol{\Upsilon}_{n-1}) + \boldsymbol{\omega}_n \\ \text{Measurement Model: } \boldsymbol{\Omega}_n = \boldsymbol{\Upsilon}_n + \boldsymbol{\varepsilon}_n \end{cases} \tag{7}$$

where $\boldsymbol{\Upsilon} = [\theta, \phi, d, v]^T$ denotes the state variable. $\boldsymbol{\Omega} = [\tilde{\theta}, \tilde{\phi}, \tilde{d}, \tilde{v}]^T$ denotes the measurement variable, as measured by the s-gNB following the radar measurement method in [11], where $\tilde{\theta}$, $\tilde{\phi}$, $\tilde{d}$ and $\tilde{v}$ represent the measured azimuth angle, elevation angle, distance and radial velocity, respectively. The terms $\boldsymbol{\omega} = [\omega_\theta, \omega_\phi, \omega_d, \omega_v]^T$ and $\boldsymbol{\varepsilon} = [\varepsilon_\theta, \varepsilon_\phi, \varepsilon_d, \varepsilon_v]^T$ are the zero-mean Gaussian noises caused by approximation and measurement, respectively. The standard Kalman Filter procedure can be employed for parameter estimation in this context.

C. Distance-based Handover

Conventional handovers are conducted through the transmission of periodic reference signals and subsequent uplink feedback about the quality of these signals after TTT. This process can result in substantial overhead, uplink and downlink signalling and extended interruption time. However, by integrating sensing capabilities into the gNB, the triggering event can be replaced with estimated parameters. Specifically, aggregated downlink slots can provide a set of measured parameters, which can then be used in a Kalman Filter (KF) to derive a corresponding set of estimated parameters. The frame structure for this sensing-assisted handover is illustrated in Fig.4.

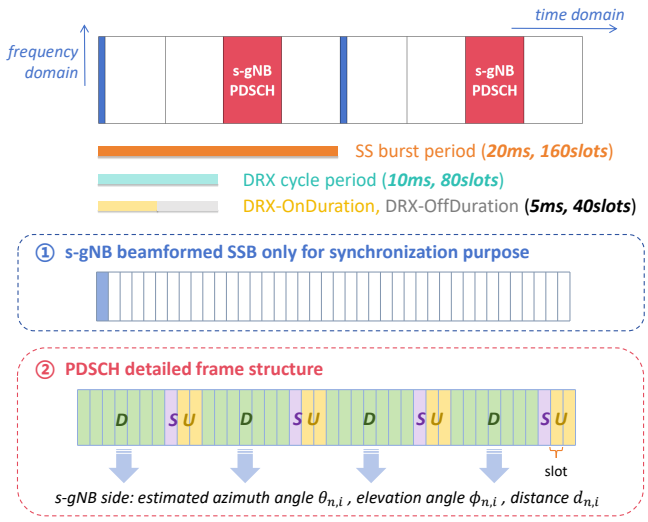

Fig. 4. Sensing-assisted Frame Structure

To be more specific, based on the frame structure proposed in Fig.4, each PDSCH block allows the gNB to take four measurements of the UE, and generate estimation parameters using the KF accordingly. This contrasts with the conventional handover frame structure, where each SS burst period only generates one time RSRP comparison. Sensing-assisted scheme thus provide four estimations of the parameters of

interest. Consequently, we introduce a new parameter, Counts-To-Trigger (CTT), to replace TTT in the sensing-assisted handover triggering scheme.

The estimated parameters of interest after KF are $\hat{\theta}_{l,i}$, $\hat{\phi}_{l,i}$ and $\hat{d}_{l,i}$, which denote the estimated azimuth angle, elevation angle and distance relative to the s-gNB at the lth PDSCH block and the ith measurement in it, where $i \in \{1,2,3,4\}$ based on the designed frame structure in Fig.4. Assuming the s-gNB has a location of $[x^{\mathrm{s}}, y^{\mathrm{s}}, z^{\mathrm{s}}]$ in the Cartesian coordinate system, the estimated location of the UE $[x^{\mathrm{u}}_{l,i}, y^{\mathrm{u}}_{l,i}, z^{\mathrm{u}}_{l,i}]$ can be expressed as:

$$\begin{cases} x^{\mathrm{u}}_{l,i} = x^{\mathrm{s}} + \hat{d}_{l,i}\cos\hat{\theta}_{l,i} \\ y^{\mathrm{u}}_{l,i} = y^{\mathrm{s}} + \hat{d}_{l,i}\sin\hat{\theta}_{l,i} \\ z^{\mathrm{u}}_{l,i} = z^{\mathrm{s}} + \hat{d}_{l,i}\sin\hat{\phi}_{l,i} \end{cases} \tag{8}$$

Assuming the location of the candidate gNB (c-gNB) $[x^{\mathrm{c}}, y^{\mathrm{c}}, z^{\mathrm{c}}]$ is known by the s-gNB, the distance between the UE and the c-gNB can be calculated as:

$$d^{\text{c-u}} = \sqrt{(x^{\mathrm{c}} - x^{\mathrm{u}}_{l,i})^2 + (y^{\mathrm{c}} - y^{\mathrm{u}}_{l,i})^2 + (z^{\mathrm{c}} - z^{\mathrm{u}}_{l,i})^2} \tag{9}$$

If $d^{\text{c-u}} < d_{l,i}$, the candidate target can be determined as t-gNB and the Distance-Triggering-Instance (DTI) can be incremented. If the s-gNB has a continuous increment of triggering-instances from the same t-gNB, and it surpasses the CTT, a handover can be triggered.

The interruption time of the sensing-based handover still includes RRC processing delay and UE processing. However, instead of waiting for the SSBs as period of the t-gNB, the t-gNB can send a beamformed SSB based on the UE's location information contained in the handover request sending from the s-gNB to the t-gNB. Additionally, instead of waiting for the first PRACH slot and sending the PRACH based on the PRACH configuration index and optimal SSB beam index, the PRACH can be also sent beamformed and immediately after the UE receives the beamformed SSB. The time occupied by RAR and RRC reconfiguration complete message remains the same as in conventional communication-only handover schemes.

Assume the maximum number of PDSCH period in interest is $L_{\max}$. The detailed steps of triggering distance-based handover can be summarized in Algorithm 1.

TABLE II
PARAMETERS OF SIMULATION

Parameter	Value	Parameter	Value
f_c	35 GHz	$L_{\max}$	155
Δf	120 kHz	ΔT	20 ms
N_t, N_r	64 (8×8)	M_r	16 (4×4)
N_{Layers}	1	Q_m	4
$N_{PRB}^{BW,\mu}$	208	T_{s}	8.929 μs
T_Δ	20 ms	$T_{\text{processing}}$	5 ms
msgA	1 slot	msgB	1 slot
msgB-ResponseWindow			4 slots
PRACH Configuration Index			$70-88$

Algorithm 1 Sensing-assisted Distance-based Handover Triggering Algorithm

Input: s-gNB, c-gNB, CTT, $L_{\max}$
Output: Handover Decision
Initialize $l \leftarrow 0$, DTI $\leftarrow 0$
for $l = 1$ to $L_{\max}$ **do**
  for $i = 1$ to 4 **do**
    Estimated parameters $\hat{\theta}_{l,i}, \hat{\phi}_{l,i}, \hat{d}_{l,i}$,
    Calculate UE coordinate $[x^{\mathrm{u}}_{l,i}, y^{\mathrm{u}}_{l,i}, z^{\mathrm{u}}_{l,i}]$ using (8)
    Calculate distance $d^{\text{c-u}}$ using (9)
    if $d^{\text{c-u}} < d_{l,i}$ **then**
      DTI $\leftarrow$ DTI $+ 1$
      if DTI $>$ CTT **then**
        Trigger HO Command
      end if
    end if
  end for
end for

IV. SIMULATION RESULTS

The simulation scenario depicted in Fig. 3 showcases a crossroad in Shenzhen, surrounded by building groups. The vehicle initially drives straight before making a left turn at the crossroad. The communication channel between the vehicle and the s-gNB comprises both LoS and NLoS paths. The s-gNB lacks prior knowledge about the vehicle's intended direction. As the vehicle traverses the crossroad, the signal quality from the s-gNB and neighboring gNBs varies, necessitating a handover. In the conventional communication-only handover, we assume the triggering event to be Event A3, with the reference signal being the periodic SS burst and the reference signal quality metric as RSRP. The offset for Event A3 is presumed to be 3dB. The frame structure of conventional communication-only scheme adheres to Fig. 1. Contrarily, the sensing-assisted handover employs a minimum distance triggering event and counts thereof, following the frame structure in Fig. 4. The initial velocity of the vehicle is set at 20m/s. Additional simulation parameters are specified in Table. II.

Fig. 5 illustrates the interruption time and HO counts for both the conventional communication-only scheme and the sensing-assisted scheme under varying TTT and CTT. The lower x-axis represents the possible choices of TTT, scaled as 10×2^xms, while the upper x-axis represents the corresponding choices for CTT. Due to the different bases, the triggering time in the sensing-assisted scheme is significantly lower than that in the conventional communication scheme. As TTT increases, the HO counts of conventional communication decrease from 2 to 1, indicating that a higher TTT makes it more challenging to trigger a handover. Furthermore, the interruption time is markedly reduced in the sensing-assisted handover compared to the conventional handover scheme. This reduction is attributed to the elimination of the need to wait for the SS burst for fine time tracking and the first PRACH

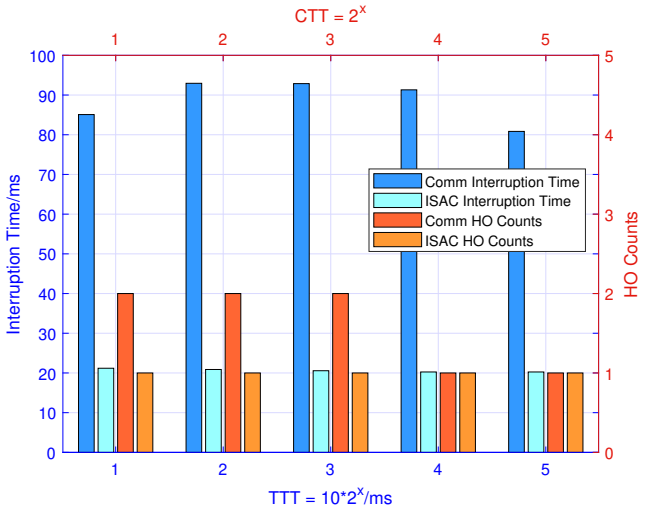

Fig. 5. Interruption time and HO counts under different TTT/CTT

occasion, which is determined by the PRACH configuration index and optimal SSB beam. Instead, the sensing-assisted handover allows the t-gNB to send a beamformed SSB beam based on the estimated UE location and await a response, thus significantly reducing the interruption time.

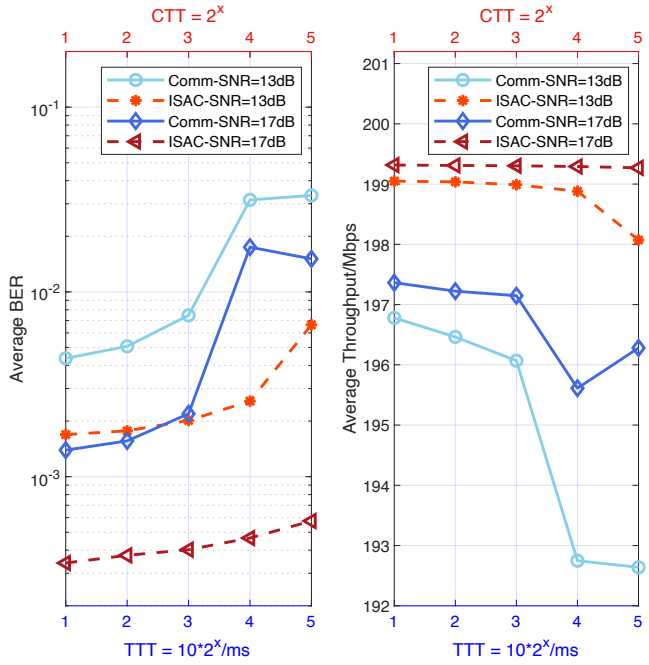

Fig. 6. BER and throughput under different TTT/CTT

In Fig. 6, we examine the relationship between bit error rate (BER), throughput and varying TTT and CTT values. As TTT/CTT increases, handover triggering is delayed, potentially resulting in higher average BER and lower throughput. The average BER and throughput of the sensing-assisted handover has consistently better performance than those of the communication-only handover, which can be attributed to three key factors. First, sensing-assisted tracking provides precise beamforming instead of relying on beam sweeping to determine optimal beam pairs from the codebook. This precise beamforming enhances the beamforming gain, thereby reducing the BER. Second, as demonstrated in Fig. 5, the interruption time and handover counts are significantly reduced in the sensing-assisted scheme, leading to increased throughput. Lastly, varying TTT/CTT values cause corresponding changes in the t-gNB selection, resulting in variations in average BER and throughput. This underscores the importance of choosing appropriate TTT/CTT values to optimize communication performance for moving targets.

V. Conclusion

In this paper, we have proposed a novel frame structure and protocol for sensing-assisted inter-cell handover in 5G NR V2I network. By integrating sensing capabilities into gNB, our proposed mechanism replaces the conventional triggering event with estimated motion parameters of the vehicle, thereby minimizing unnecessary signaling and reducing interruption time. Numerical results from link-level simulation demonstrated the effectiveness in reducing interruption time and enhancing communication performance.

References

[1] K. Abboud, H. A. Omar, and W. Zhuang, "Interworking of DSRC and cellular network technologies for V2X communications: A survey," *IEEE transactions on vehicular technology*, vol. 65, no. 12, pp. 9457–9470, 2016.

[2] S. Lu, F. Liu, Y. Li, K. Zhang, H. Huang, J. Zou, X. Li, Y. Dong, F. Dong, J. Zhu *et al.*, "Integrated sensing and communications: Recent advances and ten open challenges," *IEEE Internet of Things Journal*, 2024.

[3] F. Liu, W. Yuan, C. Masouros, and J. Yuan, "Radar-assisted predictive beamforming for vehicular links: Communication served by sensing," *IEEE Transactions on Wireless Communications*, vol. 19, no. 11, pp. 7704–7719, 2020.

[4] W. Yuan, F. Liu, C. Masouros, J. Yuan, D. W. K. Ng, and N. González-Prelcic, "Bayesian predictive beamforming for vehicular networks: A low-overhead joint radar-communication approach," *IEEE Transactions on Wireless Communications*, vol. 20, no. 3, pp. 1442–1456, 2020.

[5] Z. Du, F. Liu, W. Yuan, C. Masouros, Z. Zhang, S. Xia, and G. Caire, "Integrated sensing and communications for V2I networks: Dynamic predictive beamforming for extended vehicle targets," *IEEE Transactions on Wireless Communications*, vol. 22, no. 6, pp. 3612–3627, 2022.

[6] X. Meng, F. Liu, C. Masouros, W. Yuan, Q. Zhang, and Z. Feng, "Vehicular connectivity on complex trajectories: Roadway-geometry aware ISAC beam-tracking," *IEEE Transactions on Wireless Communications*, vol. 22, no. 11, pp. 7408–7423, 2023.

[7] S. Bin Iqbal, S. Nadaf, U. Karabulut, P. Schulz, A. Prado, G. P. Fettweis, and W. Kellerer, "On the mobility analysis of UE-ide beamforming for multi-panel user equipment in 5G-Advanced," in *2023 IEEE 34th Annual International Symposium on Personal, Indoor and Mobile Radio Communications (PIMRC)*, 2023, pp. 1–7.

[8] L. Sun, J. Hou, and T. Shu, "Optimal handover policy for mmwave cellular networks: A multi-armed bandit approach," in *2019 IEEE Global Communications Conference (GLOBECOM)*. IEEE, 2019, pp. 1–6.

[9] 3GPP, "NR; Radio Resource Control (RRC); Protocol specification," 3rd Generation Partnership Project (3GPP), Technical Specification (TS) 38.331, 2023, version 17.4.0.

[10] ——, "NR; Requirements for support of radio resource management," 3rd Generation Partnership Project (3GPP), Technical Specification (TS) 38.133, 2023, version 18.1.0.

[11] Y. Li, F. Liu, Z. Du, W. Yuan, Q. Shi, and C. Masouros, "Frame structure and protocol design for sensing-assisted NR-V2X communications," *IEEE Transactions on Mobile Computing*, 2024.